JPhys Materials

TOPICAL REVIEW • OPEN ACCESS

How photoluminescence can predict the efficiency of solar cells

To cite this article: Susanne Siebentritt *et al* 2021 *J. Phys. Mater.* **4** 042010

View the article online for updates and enhancements.

You may also like

- Model-Assisted 4-Electrode Cell Design for Li-Based Electrolyte Characterization
Mohammad Farkhondeh, Mark Pritzker, Michael Fowler et al.
- Deep-Discharge Performance of Lead Acid Battery Using Graphite Based Composite As Cathode Current Collector
Kaito Sugimoto, Yuta Hano, Hiroshi Okano et al.
- Analysis of Local Dissolution Behavior of Intermetallic Particles on Chromate-Treated AA1050 Using Micro-Electrochemical System
Hiroshi Kakinuma, Izumi Muto, Yoshiyuki Oya et al.

This content was downloaded from IP address 93.12.247.50 on 18/01/2022 at 12:34

IOP Publishing J. Phys. Mater. 4 (2021) 042010 https://doi.org/10.1088/2515-7639/ac266e

Journal of Physics: Materials

OPEN ACCESS

RECEIVED
29 July 2021

REVISED
27 August 2021

ACCEPTED FOR PUBLICATION
14 September 2021

PUBLISHED
7 October 2021

Original content from this work may be used under the terms of the Creative Commons Attribution 4.0 licence.

Any further distribution of this work must maintain attribution to the author(s) and the title of the work, journal citation and DOI.

TOPICAL REVIEW

How photoluminescence can predict the efficiency of solar cells

Susanne Siebentritt[1,*], Thomas Paul Weiss[1], Mohit Sood[1], Max Hilaire Wolter[1], Alberto Lomuscio[1,2] and Omar Ramirez[1]

[1] Laboratory for Photovoltaics, Department of Physics and Materials Science, University of Luxembourg, Belvaux, Luxembourg
[2] Avancis GmbH, Munich, Germany
[*] Author to whom any correspondence should be addressed.

E-mail: susanne.siebentritt@uni.lu

Keywords: solar cells, photoluminescence, radiative efficiency, interface recombination, diode factor

Abstract

The efficiency of solar cells depends on the photocurrent, on the open circuit voltage and on the fill factor, which in turn depends on the diode factor. We review how photoluminescence (PL) measurements on the absorber, without finishing the solar cell, reveal the maximum open circuit voltage and the best diode factor, that can be reached in the finished device. We discuss two different ways to extract the quasi Fermi level splitting (QFLS) from absolute calibrated PL spectra, measured at a one sun excitation. The absorption spectrum of the solar cell absorber can be extracted from the PL spectra and allows the reliable determination of tail states. Tail states are responsible for radiative and non-radiative losses in the QFLS. In the ideal case the open circuit voltage is given by the QFLS. However, recombination at the interface can reduce the open circuit voltage severely. We discuss various electronic structures at the interface that lead to a reduction of the open circuit voltage. The excitation dependence of the PL allows the determination of the diode factor of the absorber alone, which would be 1 in the ideal case. Metastable defects can increase the diode factor, even for recombination in the neutral zone and for low excitation. This effect decreases the fill factor of the solar cell.

1. Solar cells and photoluminescence

Thin film solar cells represent the electricity source with the lowest greenhouse gas emissions [1]. Two technologies have reached confirmed efficiencies in the lab above 23% [2–4]: $Cu(InGa)Se_2$ and halide perovskites, with CdTe closely behind with 22.1% efficiency [2]. Thin film solar cells are complex structures, consisting of many layers and their interfaces. For the solar cell to work all materials and interfaces need to possess the appropriate electronic structure. During the development of solar cells or in industrial production, it is desirable to know already the quality of the absorber alone. Photoluminescence (PL) measurements of the absorber can provide information about the open circuit voltage [5] and the fill factor, which the absorber is able to produce when made into a solar cell. The open circuit voltage of a solar cell with ideal contacts and with ideal transport properties is given by the quasi Fermi level splitting (QFLS) of the absorber under one sun illumination [6, 7]. The fill factor of a solar cell depends critically on the diode factor of the device. We discuss in the following how PL can determine the diode factor of the absorber. It should be pointed out that these PL measurements are done at room temperature, not a cryogenic temperatures. We want to describe the absorber as close as possible to standard test conditions of the solar cell. Furthermore, room temperature PL measurements are more easily implemented in an industrial environment. Most of our examples come from chalcopyrite solar cells, but the principles are generally applicable to any solar cell technology.

2. QFLS

The QFLS is a measure for the open circuit voltage, because the latter is given by the difference between the quasi Fermi level of the conduction band at the electron contact and the quasi Fermi level of the valence band

© 2021 The Author(s). Published by IOP Publishing Ltd

at the hole contact. Without gradients in the quasi Fermi levels at open circuit, the QFLS translates directly into the open circuit voltage as $V_{OC} = \Delta E_F/q$ (symbols are explained in the annex). However, in real solar cells, the contacts are not ideal and gradients in the quasi Fermi levels can form (see section 4), reducing the open circuit voltage[3]. Thus, the QFLS gives the maximum open circuit voltage an absorber is capable of.

In equilibrium any semiconductor emits black body radiation. Since a semiconductor is a grey body with a certain absorption spectrum, we need to multiply the black body emission with the absorptance of the semiconductor film or wafer [9, 10]. Thus, the photon emission flux is given by:

$$\Phi_{eq}(E) = A(E)\Phi_{BB}(E) \approx A(E)\frac{E^2}{4\pi^2\hbar^3c^2}e^{-E/k_BT}, \tag{1}$$

where we use the Boltzmann approximation instead of the Bose term in Planck's law for black body radiation. This is allowed [11] since we are interested in the band edge luminescence of semiconductors which are used in solar cells, i.e. have a band gap and therefore emission energies much larger than k_BT. Two things are important to point out: (a) Φ and F, below in equation (2), describe the (external) photon flux, not the (internal) recombination rate, (b) A is the absorptance, i.e. the ratio of absorbed photons to incident photons, not the absorption coefficient, i.e. it depends also on the thickness of the semiconductor film or wafer [9]. This emission flux is caused by the recombination of thermally excited carriers. Thus, the spectrally integrated emission flux is given by the concentration of electrons and holes:

$$F_{eq} = \int \Phi_{eq}(E)dE = B \times np = B \times n_i^2. \tag{2}$$

Under excitation by the sun or by a laser, the carrier concentrations increase, which is described by the QFLS:

$$F_{PL} = B \times np = B \times n_i^2 e^{\Delta E_F/k_BT}. \tag{3}$$

Combining equations (1)–(3) gives the photon flux under excitation, assuming a constant QFLS throughout the absorber:

$$\begin{aligned}\Phi_{PL}(E) &\approx A(E)\Phi_{BB}(E)e^{\Delta E_F/k_BT} \\ &\approx A(E)\frac{E^2}{4\pi^2\hbar^3c^2}e^{-(E-\Delta E_F)/k_BT}.\end{aligned} \tag{4}$$

For a detailed derivation, that applies also to the energy range where the Boltzmann approximation is not valid, see [9]. Equation (4) is also known as Generalised Planck's law (in Boltzmann approximation). A fit of the PL spectrum to equation (4) can be used to determine the QFLS. The usual method [12, 13] assumes that the absorptance is 1 at energies high enough above the bandgap. Then a logarithmic plot of Φ/E^2 results in a straight line at energies well above the bandgap, i.e. well above the PL maximum energy, with the slope proportional to the inverse temperature at which the measurement was taken and the ordinate intercept given by the QFLS (see e.g. supplementary information of [14]). An example is given in figure 1. If the fitted temperature does not agree with the measurement temperature care needs to be taken, since a wrong temperature results also in a wrong QFLS from the fit [15]. Quite often, increased temperatures are reported in the literature, even above 100 °C. However, it is not very likely that the temperature increases considerably above room temperature during a measurement at one sun equivalent illumination, in particular if the measurement is done at a mm sized spot on a thin film absorber with a conductive back contact. Whether the ratio of non-radiative to radiative recombination is low or high has negligible influence on the temperature, since the highest radiative efficiency in the best solar cells is only 20% (see figure 2), i.e. even in the best case, non-radiative recombination is already responsible for 80% of the recombination. We check the temperature increase with the help of an infrared thermometer camera, that allows to check if the surface temperature in the laser spot is higher than the surrounding. We only see small temperature differences, usually below 5 K, and only if the illumination intensity is equivalent to several suns. The likely reason to observe a seemingly increased temperature is that the assumption of $A = 1$ is not valid. In some cases it is possible to obtain an acceptable fit, fixing the temperature parameter to the measurement temperature; then the intercept will result in the correct QFLS. If fixing the temperature does not result in a reasonable fit, the assumption of $A = 1$ can no longer be maintained. The absorptance above the band gap has to be determined by absorption–reflection or ellipsometry measurements and a fit to equation (4) using the

[3] Away from V_{OC}, where currents flow, a significant difference between the voltage and the QFLS can occur, even for almost ideal contacts [8]. Here, we concentrate on the open circuit case.

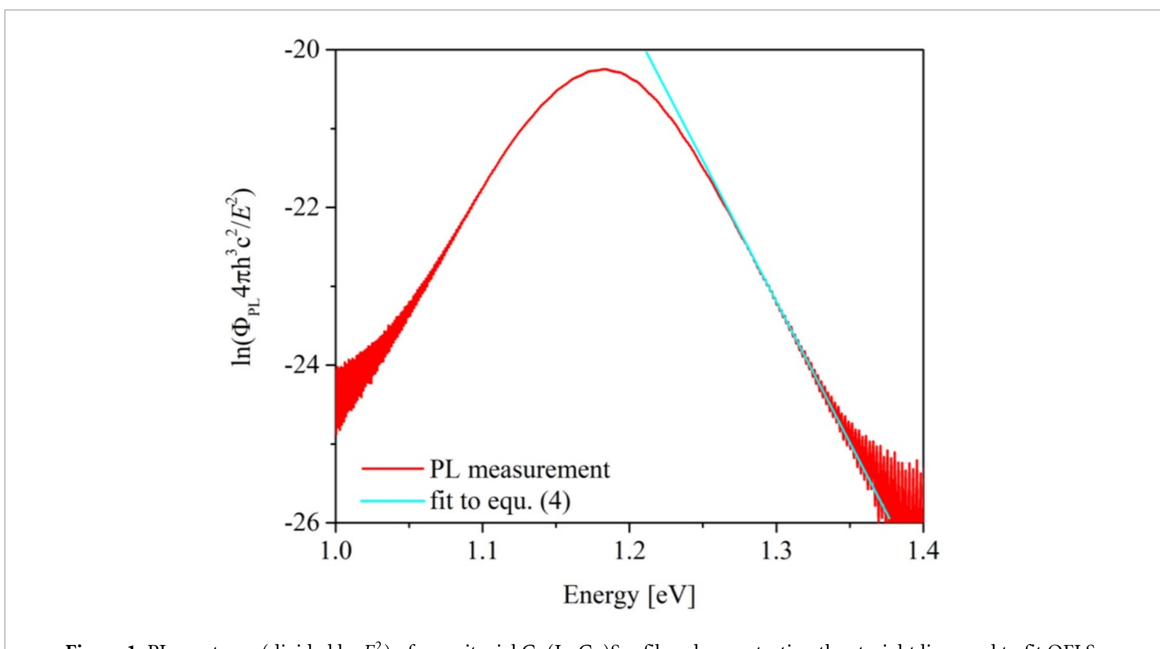

Figure 1. PL spectrum (divided by E^2) of an epitaxial Cu(In,Ga)Se_2 film, demonstrating the straight line used to fit QFLS.

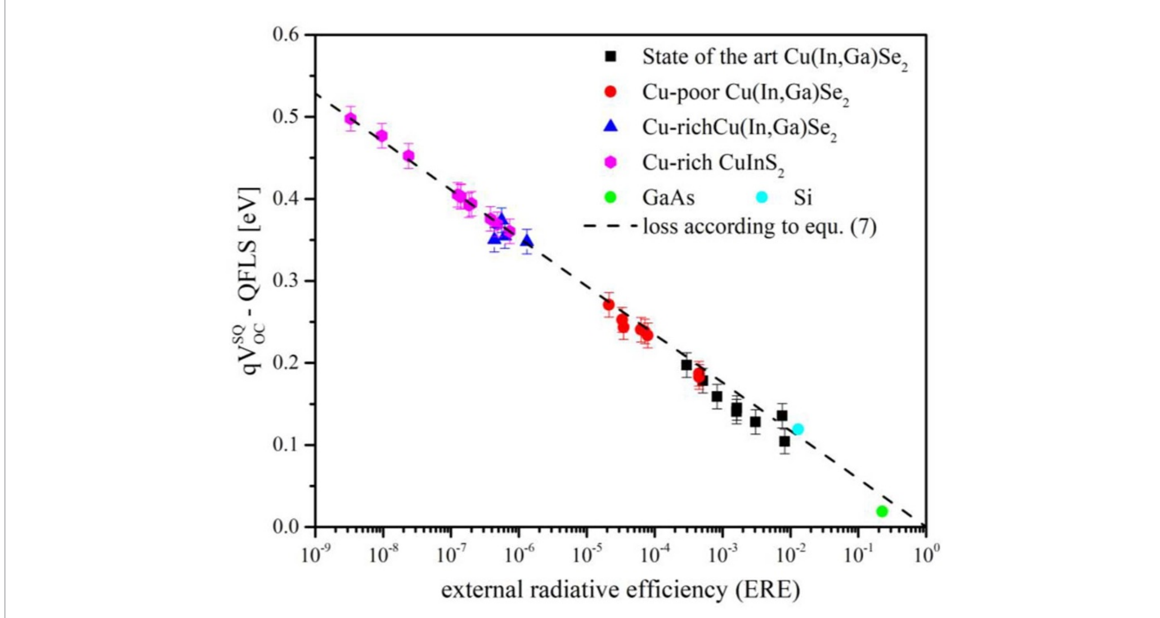

Figure 2. QFLS loss, determined from a fit to the PL spectrum vs ERE, illustrating the dependence of equation (7), represented by the dashed line. V_{OC} loss of record solar cells is added.

experimentally determined absorptance spectrum will reveal the correct QFLS [15]. Alternatively, the QFLS can be determined not by the fit but by the external radiative efficiency (ERE), also known as PL quantum efficiency or PL quantum yield, as discussed in the following.

Consider first an ideal solar cell at open circuit. The ideal solar cell is governed by the detailed balance between excitation and radiative recombination, as described by Shockley and Queisser [6], resulting in a QFLS of $\Delta E_F = qV_{OC}^{SQ}$. Combining equations (2) and (3) gives the emission flux due to radiative recombination which is balanced by the excitation flux from the sun and the thermal radiation form the environment

$$F_{PL} = F_{eq}e^{qV_{OC}^{SQ}/k_B T} = G_{sun} + F_{eq} \tag{5}$$

where it is understood that G_{sun} is the photon flux from the sun, integrated for energies above the bandgap of the absorber. Obviously, in a PL experiment the photons are not supplied by the sun but by a laser tuned to the photon flux that is contained in the sun's spectrum above the band gap of the absorber. The thermal

photon flux F_{eq} on the right hand side is essential for the derivation of the current–voltage characteristics of a solar cell [6], but can be neglected for the consideration at open circuit. In a real solar cell non-radiative recombination is the dominant recombination mechanism, which reduces the number of photogenerated carriers, and therefore the QFLS and V_{OC}. Furthermore, the flux of emitted photons is reduced by F_{nr}. Thus, the balance is between [6]:

$$F_{PL} + F_{nr} = F_{eq}e^{\Delta E_F/k_BT} + F_{nr} = G_{sun} = F_{eq}e^{qV_{OC}^{SQ}/k_BT} = \frac{F_{PL}}{ERE}. \tag{6}$$

The second line is valid since ERE is defined as F_{PL}/G_{sun}. Solving equation (6) for the QFLS gives [6]

$$\Delta E_F = qV_{OC}^{SQ} + k_BT\ln ERE. \tag{7}$$

To extract the QFLS from ERE, the value V_{OC}^{SQ} is needed. It can be determined by solving equation (5) for V_{OC}^{SQ}. This requires information on the band gap, since G_{sun} depends on the band gap of the absorber, for tabulated values see e.g. [16]. The band gap can be determined from absorption–reflection or ellipsometry measurements and a Tauc plot [17, 18] or from the inflection point of the quantum efficiency spectrum of the solar cell [19]. Since the Shockley–Queisser model assumes complete absorption above the band gap, equation (5) is valid independent of a direct or indirect band gap. The V_{OC}^{SQ} values determined from equation (5) changes, whether a 6000 K black body spectrum is used [6] or an AM1.5 spectrum, because this changes the value of G_{sun}, and whether a model with or without ideal back reflector is applied, because this changes the value of F_{eq} [16]. It is important to note that it is the ERE that enters into equation (7), because in the Shockley–Queisser limit the fluxes of photons (not the internal recombination rates) have to be considered [6, 7]. Essentially, the photons that do not leave the absorber will be re-absorbed and then mostly lost to non-radiative recombination [20].

A comparison between QFLS extracted from a fit with fixed temperature to the high energy slope of the PL spectrum and the ERE, both obtained from the absolute calibrated PL measurement, is given in figure 2. We plot the QFLS loss with respect to V_{OC}^{SQ}, calculated for an AM1.5 spectrum and without back reflector, using the PL maximum energy as the band gap. We compare a number of chalcopyrite solar cells in different stages of development. The state of the art $Cu(InGa)Se_2$ solar cells were prepared by EMPA, the Swiss research institute on Materials Science and Technology, and ZSW, the Zentrum für Sonnenenergie- und Wasserstoff-Forschung Baden-Württemberg, and have been published before [21, 22]. Cu-rich and Cu-poor $Cu(InGa)Se_2$ solar cells are described in [14] and the sulphide $CuInS_2$ solar cells in [23]. We added literature data for Si and GaAs record cells. Here we use V_{OC} instead of QFLS. For these cells no ERE data is available. Therefore we used the reciprocity principle [24] to estimate ERE from the published external quantum efficiency (EQE) data [25]. The data for the Si cell are taken from [26] and for the GaAs cell from [27]. The data in figure 2 confirms that the correlation of equation (7) is observed, implying that all these solar cells can be described by detailed balance plus non-radiative recombination. This has also been shown in the literature, see e.g. [7, 24, 28]. The loss in state of the art $Cu(In,Ga)Se_2$ cells and the GaAs record cell is somewhat lower than the line. This is due to the fact that these optimised cells are closer to a perfect back reflector and have therefore a higher V_{OC}. An important point to notice is that the ERE, even in the best solar cells is below 30%. Thus, the dominating recombination is still non-radiative—in general not due to bad material quality, but due to imperfect light management [29]. Experimentally, QFLS can be determined by both methods: from a fit to the spectrum, provided the fitted temperature is not wrong, or from EQE with the help of equation (7).

Obviously, to perform these analyses we need the photon flux, i.e. we need to calibrate the PL measurements for photon counting. This absolute calibration is achieved by two steps. (a) Spectral calibration: the spectral throughput of all optical components between the sample and the detector is measured with the help of a calibrated lamp with a known spectrum. A white spectralon reflector is placed at the exact position of the sample to be measured, the lamp is reflected into the detection system and the spectrum measured. The ratio between the calibrated lamp spectrum and the spectral counts of the detector gives the spectral correction function. (b) Intensity calibration is performed at a (reduced) laser power equivalent to the (expected) PL intensity by first placing a power meter at the sample position and measuring the laser power. Then a camera is placed in the same position to determine the laser profile and, thus, the intensity in the centre, where the PL is measured. Finally, the spectralon reflector is placed again at the sample position and the laser reflected through the whole optical system to the detector, which allows to determine the factor between (spectrally corrected) counts and intensity or number of photons.

QFLS depends on both quasi Fermi levels. The minority quasi Fermi level depends on the concentration of photo excitated carriers, i.e. on excitation and recombination. The majority quasi Fermi level depends on

the doping level in low excitation and on the density of photo excited carriers in high excitation. For most doped absorbers, one sun illumination is still low excitation. In this case the behaviour of the quasi Fermi levels can be approximated in the following way: only the minority carrier quasi Fermi level is shifted by the excitation and the majority carrier quasi Fermi level is given by the equilibrium Fermi level. The cases beyond this approximation are discussed in section 6. For the simulation of an example see [30]. Comparing two samples, a higher QFLS can mean (a) reduced recombination activity and thus a minority carrier quasi Fermi level closer to the band or (b) a higher doping level and thus a majority quasi Fermi level closer to the band [13, 31]. To separate the two effects, time resolved PL measurements are needed, which in principle allow the determination of the minority carrier lifetime. The influence of varying experimental conditions and the potential effects that could distort the result can be found in the literature [32–34]. If the reduction of recombination centres has a considerable effect on the QFLS, when comparing two samples, then the minority carrier lifetime will be increased. The effect on QFLS can be approximated by assuming that the carriers have a reasonably good mobility and spread evenly over the thickness of the absorber during the steady state QFLS measurement, an assumption already made when deriving equation (4). Then the minority carrier density is given by $n_{\min} = G \cdot \tau / d$. Comparing two (otherwise similar) samples the expected change in QFLS due to a change in minority carrier lifetime is then given by

$$\Delta\left(\Delta E_{\mathrm{F}}\right) = k_{\mathrm{B}} T \ln\left(\tau_1/\tau_2\right). \tag{8}$$

If the main effect leading to the QFLS improvement is an increase in doping level, the minority carrier lifetime remains unchanged [31]. The doping level can be cross-checked by Hall measurements (for methods how to deal with low mobility samples, see [35, 36]) or by capacitance–voltage measurements on finished devices [37, 38]. In most cases, both effects will play a role and the improvement in QFLS will exceed the one expected from an increase in lifetime, as given in equation (8).

3. Tail states

To determine the QFLS from the ERE (equation (7)), the band gap of the absorber is needed. The determination of the band gap can be severely hampered by tail states [39]. In an ideal semiconductor the density of states in the band gap is zero. However, in real semiconductors, and in particular in polycrystalline thin films, band tails occur, which are characterised by a density of states decaying exponentially into the gap. The decay constant is called the Urbach energy [40–43]. Essentially, higher Urbach energies mean there are more tail states. Exponential tail states have been first described in metal halides by Urbach, who also discovered the temperature dependence of the decay energy [44], which is now known as Urbach energy. The temperature dependence of the Urbach energy can be attributed to the vibrational disorder caused by phonons, while static disorder adds an additional constant contribution [41, 45]. The static disorder can be due to structural deviations from the ideal crystal, e.g. grain boundaries, due to variations in the composition, and thus the band gap [46] or due to electrostatic fluctuations [47, 48]. These bandgap or electrostatic fluctuations are characterised by low temperature PL spectra [49–53], which show a characteristic temperature dependence and spectral shape: the spectrum is asymmetrically broadened towards lower energies because non-local transitions allow recombination at lower energies than locally vertical ones. The peak maximum shifts first towards lower energies as the temperature is increased, because carriers become mobile and find the lowest energy states. With further temperature increase more thermal carriers are available, which flattens the electrostatic potential differences or fills the low energy states, so that the PL peak shifts towards higher energies with increasing temperature [54].

However, it is the density of states at room temperature that is relevant for the solar cell performance and is characterised by Urbach energy. The Urbach energy is determined from the exponential behaviour of the absorption coefficient below the band gap. For an accurate determination of the Urbach energy, the measurement of very low absorption coefficients is necessary to describe the states deep in the gap [55, 56]. Since in general it is easier to detect single emitted photons than to detect missing photons, PL is particularly suited to measure ultra-low absorption coefficients [57]. The emission flux of an excited semiconductor contains the absorptance spectrum of the sample (equation (4)). With the knowledge of the QFLS the spectrum of the absorptance can be extracted from the emission spectrum. Since the emission spectrum extends over energies lower than the band gap up to about 100 meV above the band gap, the extracted absorption spectrum also covers this range. The lower energy limit is generally given by the detector. Using an optical model for the sample, the absorption coefficient can be extracted [15]. The original method [57] was developed for wafers, we have expanded the method to be used for thin films [15]. The method has been confirmed by comparison with the more classical method of photothermal deflection spectroscopy (PDS), which has been particularly developed to measure low absorption coefficients [58]. In fact, PL allows to

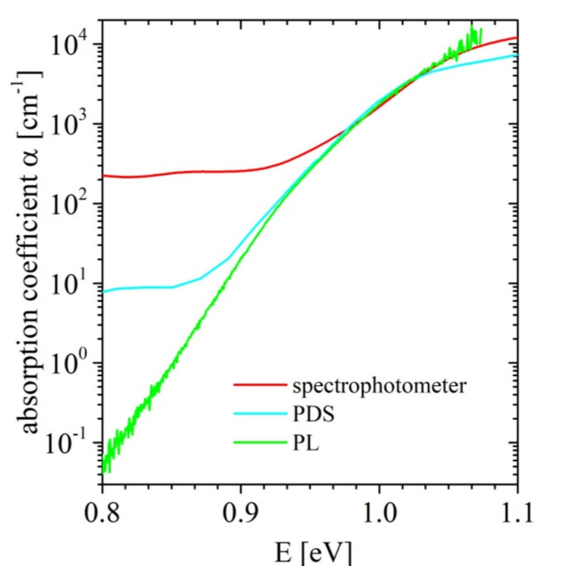

Figure 3. Absorption coefficient of a polycrystalline $CuInSe_2$ sample, showing the exponential tail states, measured by transmission and reflection in a spectrophotometer, by photo deflection spectroscopy (PDS) or by photoluminescence (PL). PL allows the measurement of the lowest absorption coefficient values. Reproduced from [15]. CC BY 4.0.

measure absorption coefficients lower than PDS by more than two orders of magnitude (see figure 3) [15]. For a reliable determination of Urbach energies it is essential to measure down to very low absorption coefficients, deep in the band gap, otherwise a possible additional variation in the band gap can distort the result [47].

Several methods exist to determine the bandgap or the effective bandgap in the case of tail states [7, 19]. In an ideal (direct) semiconductor the maximum of the PL emission is given by the band gap: $E_G + k_B T/2$ (see e.g. [59]). In the presence of tail states, the excited carriers will thermalise not only down to the edges of the extended band states but further into the tail states [60]. Thus, the maximum of the emission spectrum will also shift to lower energies, more so for less steep tails, as observed in a wide range of materials [7, 39]. Since the detailed balance in the Shockley–Queisser limit is determined by the radiative recombination, the QFLS is limited in the best case by the energy of the emitted photons. Therefore, to determine the qV_{OC}^{SQ} in equation (7) we use the maximum of the PL emission spectrum as the band gap energy [39]. This shift of the PL maximum represents an additional radiative loss of QFLS and thus V_{OC} due to tail states. However, the additional density of states also broadens the absorption and with it the luminescence spectrum towards lower energies, thereby increasing F_{eq} (equation (2)). Because of equation (5) this will reduce the maximum open circuit voltage even in the radiative case [7, 60]. We label this reduced open circuit voltage V_{OC}^{rad}. This loss is significant, even for rather low Urbach energies (lower than $k_B T$): the loss increases by 5 meV for each increase of 1 meV in the Urbach energy [60]. An equally high additional loss is due to the non-radiative Shockley–Read–Hall (SRH) recombination through the tail states [60]. Thus, the V_{OC} loss due to tail states is significant: leading at least to an additional V_{OC} loss of 10 mV for every additional meV in Urbach energy.

4. Interface recombination

So far, we have treated V_{OC} and QFLS almost as synonyms. QFLS and V_{OC} are reduced from the radiative limit qV_{OC}^{SQ} by non-radiative recombination processes, reducing ERE and the minority carrier lifetime from its ideal radiative value. These recombination processes take place in the bulk of the absorber and at the interfaces [5, 61]. In general, good solar cells are dominated by bulk recombination [62, 63]. However, it should be noted, that the interface is always a location of defects and recombination centres. Consequently, as the quality of the absorber is improved towards the radiative limit, eventually for the best bulk, interface recombination will be the limiting factor again. On identical absorbers the quality of the interface can be inferred from QFLS and lifetime measurements [61, 63]: with stronger interface recombination the effective minority carrier lifetime is reduced and consequently the QFLS is reduced (equation (8)). However, the influence of interface recombination on solar cell performance can go much beyond the reduction of QFLS. Interface recombination can cause a gradient in one (or both) of the quasi Fermi levels, typically in the minority carrier quasi Fermi level. Since the (open circuit) voltage is given by the difference between the

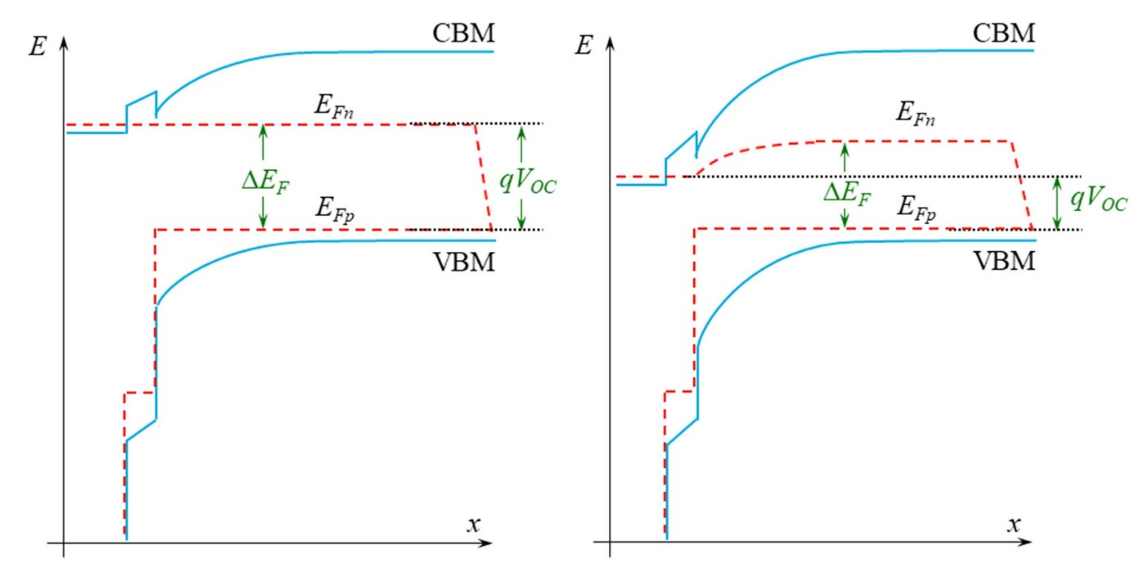

Figure 4. Quasi Fermi level gradient at open circuit—the example of a chalcopyrite solar cell: with an ideal interface the open circuit voltage is given by the quasi Fermi level splitting (left). Interface recombination (right) represents an additional recombination channel and thus reduces the quasi Fermi level splitting. More importantly, it introduces a gradient in the minority quasi Fermi level and reduces the open circuit voltage even more. [64] John Wiley & Sons. © 2018 The Authors. Solar RRL Published by WILEY-VCH Verlag GmbH & Co. KGaA, Weinheim.

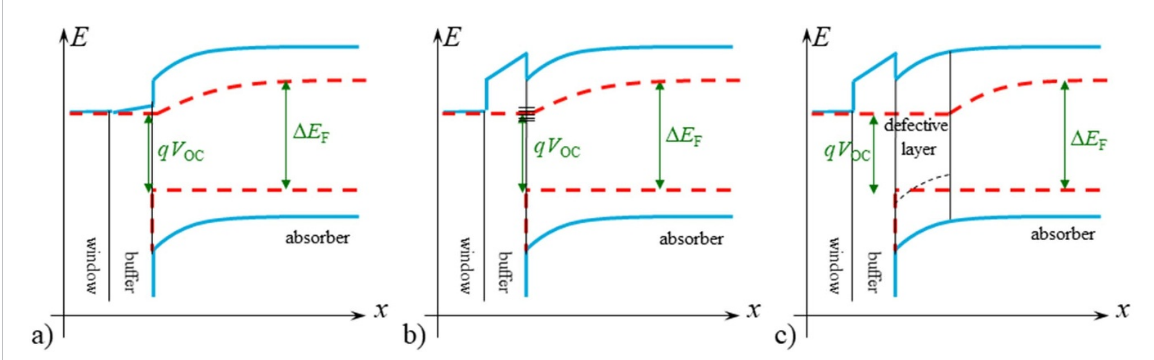

Figure 5. Different interface electronic structures that lead to interface recombination with an activation energy of the saturation current smaller than the band gap and an additional ΔV_{OC}^{IF} loss: cases (i)–(iii) as discussed in the text. Reproduced from [65]. CC BY 4.0.

electron quasi Fermi level at the n-contact and the hole quasi Fermi level at the p-contact, such a gradient will reduce the open circuit voltage, see figure 4 [64]. Therefore we define the interface open circuit loss as the difference between QFLS and open circuit voltage, both measured under one sun illumination [65]:

$$\Delta V_{OC}^{IF} = \Delta E_F/q - V_{OC}. \tag{9}$$

In state of the art solar cells with optimised interfaces this loss is small, less than 10 mV [22, 63].

Whether interface recombination is the dominating loss mechanism at V_{OC} can also be studied by temperature dependent current–voltage measurements. The activation energy of the dominating recombination rate in a solar cells is given by the activation energy E_a of the reverse saturation current and can be determined from the temperature dependence of the open circuit voltage by extrapolating to 0 K:

$$V_{OC} = \frac{E_a}{q} - \frac{n_d k_B T}{q} \ln\left(\frac{j_{00}}{j_{SC}}\right). \tag{10}$$

Equation (10) is obtained by solving the diode equation under illumination for the open circuit voltage (see e.g. [62]). If the dominating recombination occurs in the bulk of the absorber, either in the neutral zone or in the space charge region, the activation energy is given by the band gap. Interface recombination can lead to a lower activation energy of the dominant recombination process. This reduction can be caused by several effects (figure 5): (i) unsuitable band alignment, causing an interface band gap smaller than the bulk band gap (ii) Fermi level pinning at the interface (iii) a defect layer within the absorber just below the surface [65].

Case (i) and (ii) are well established causes of dominating interface recombination and are discussed in detail in textbooks (e.g. [62, 66]). In the case of unsuitable band alignment (i) (figure 5(a)) one of the band edges of the contact material is energetically situated within the band gap of the absorber. This is labelled as cliff. The interface band gap is then reduced, as it is defined by the closest energetic distance between a valence band and a conduction band at the interface. This energetic distance is the relevant energy, because recombination across the interface is possible, i.e. electrons of one material recombine with holes from the other one [62]. This smaller interface bandgap leads to a reduced activation energy of the saturation current—and consequently to increased recombination—because recombination will occur between the lowest energy electrons and the highest energy holes on either side of the interface. If the band alignment is suitable, i.e. the band edges of the contact material lie outside the band gap of the absorber (type I), a high density of interface states can lead to Fermi level pinning (ii) (figure 5(b)). In this case the activation energy is expected to be given by the energetic distance between the (equilibrium) Fermi level and the (bulk) majority band edge at the interface (i.e. the valence band edge for a p-type absorber) [67]. Recent device simulations [65] show, that this is a useful approximation. However, in several cases an activation energy of the saturation current lower than the band gap has been observed, that is not due to unfavourable band alignment, nor does any hint exist from e.g. photoemission experiments, that Fermi level pinning occurs [65, 68–70]. We recently showed [65] that a highly defective layer with a thickness of a few 10 nm just below the surface (iii) (figure 5(c)) will also lead to a significant gradient in the minority carrier quasi Fermi level, i.e. to a large interface V_{OC} loss (equation (9)). In particular, the current voltage characteristics show the most important indicator of interface recombination: an activation energy of the saturation current smaller than the band gap. Thus, it would be more correct to say that this observation indicates recombination **near or** at the interface.

Chalcopyrite solar cells are particularly well suited to study the influence of interface recombination, because in general they show bulk recombination, when the absorber is grown under Cu-poor conditions, and interface recombination when it is grown under Cu-rich conditions [68, 69, 71–73]. In particular, Cu-rich absorbers show interface recombination even with a buffer material that ensures suitable band alignment [69, 74]. In devices with suitable buffers the activation energy of the saturation current equals the band gap in Cu-poor devices and is lower than the band gap in Cu-rich devices. Furthermore, in Cu-poor devices with optimised contact layers the interface V_{OC} loss ΔV_{OC}^{IF} is small, less than 10 mV [22]. In Cu-poor devices with non-optimised contacts we find ΔV_{OC}^{IF} of up to 60 mV [14], although the current voltage characteristics give no hint on interface recombination. In this case, additional gradients of the quasi Fermi levels exist within the contact layers, which is a hint that the transport properties of the contact layers need to be improved. But ΔV_{OC}^{IF} is considerably larger in Cu-rich devices, values around 150 mV are typical in selenides [14, 65] and above 300 mV in sulphides [72]. Such large values of ΔV_{OC}^{IF} (>100 mV) have always been found in conjunction with an activation energy of the saturation current smaller than the band gap. This is why we label the loss defined in equation (9) *interface* V_{OC} loss. Large values indicate interface recombination, either because of unfavourable band alignment, Fermi level pinning or a defective layer just below the surface.

5. Summary of Voc losses

Figure 6 summarises the losses that can occur in a solar cell to reduce the open circuit voltage.

For a given band gap V_{OC}^{SQ} represents the maximum open circuit voltage for idealised absorption assumptions and radiative recombination as the only recombination mechanism. If the material contains considerable tail states the energy of the radiative recombination E_{PL} is reduced with respect to the band gap. This shift of the radiative recombination leads already to a loss of the open circuit voltage, even in the case of purely radiative recombination, and leads to V_{OC}^{rad}. Non-radiative recombination due to SRH recombination through deep defects or through tail states reduces the QFLS ΔE_F below the value for only radiative recombination. This includes non-radiative recombination at the interface. However, interface recombination leads to an additional gradient of the minority quasi Fermi level towards the interface and therefore to an open circuit voltage that's even lower than the (bulk) QFLS.

PL spectroscopy provides a lot of this information: the amount of tail states allows to calculate V_{OC}^{rad}. Absolute calibrated PL spectra allow to extract the QFLS. Finally, the difference between V_{OC} and $\Delta E_F/q$ gives the extend of interface losses.

6. Higher diode factor losses due to metastable defects

In addition to elucidating the various sources of voltage losses, PL spectroscopy can also help to identify fill factor losses. The fill factor of a solar cell depends on the parasitic resistances (see e.g. [75]). To optimise

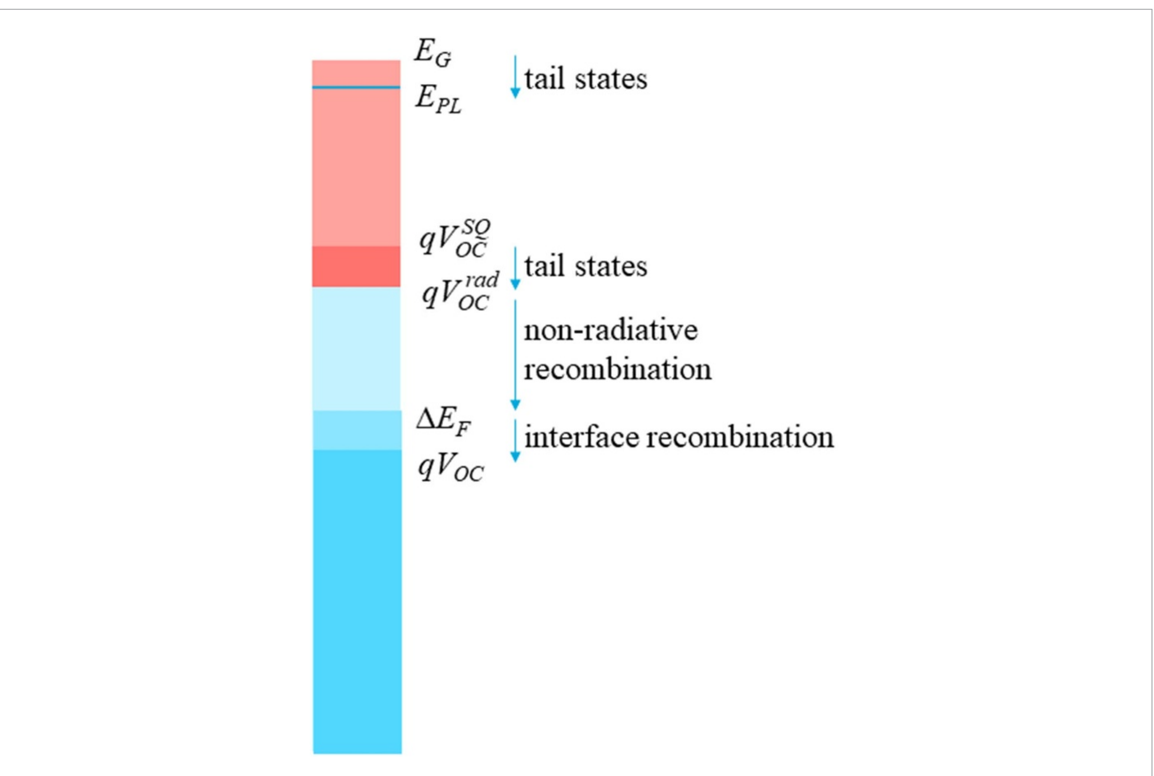

Figure 6. Summary of open circuit voltage losses. Red colours describe the ideal state and blue colours the quantities relevant for real solar cells. The different effects are explained in the text.

them is a matter of device design. Here we concentrate on the fundamental influences that originate from the absorber material itself. The fill factor depends also critically on the diode factor of the cell (n_d in equation (12) below, see e.g. [62]), which in turn depends on the main recombination mechanism [62]. Ideally the diode factor is 1. Higher diode factors will lead to lower fill factors and consequently to lower efficiencies of the solar cell. In devices that are dominated by recombination in the quasi-neutral zone the diode factor can be determined from PL measurements, since PL is measured on the absorber alone, therefore no space charge region exists [64]: experimentally a power law is found between the generation flux and the PL flux (e.g. [76] and references therein):

$$F_{\mathrm{PL}} \sim G^k. \tag{11}$$

Examples are given in figure 7, which shows a log plot of the PL flux as a function of the generation flux, resulting in a straight line over four orders of magnitude with an exponent of 1.2–1.4. On the other hand the current–voltage characteristics of the solar cell depends on the diode factor n_d. Neglecting parasitic resistances it can be written:

$$j = j_0\left(\mathrm{e}^{qV/(n_d k_B T)} - 1\right) - j_{SC} \Leftrightarrow j_{SC} \approx j_0 \mathrm{e}^{qV_{OC}/(n_d k_B T)}. \tag{12}$$

Because the generation flux G is proportional to the short circuit current of a solar cell and because the luminescence flux is given by equation (5) and because with good contacts the open circuit voltage is given by the QFLS, the exponent k and the diode factor n_d of the current–voltage characteristics are the same [64, 77]. Therefore, the exponent k is labelled the optical diode factor [64]. $k = n_d$ is true in devices that are dominated by recombination in the quasi-neutral zone. Devices that are dominated by recombination in the space charge region or at the interface will have a diode factor $n_d \geqslant k$ [64]. Thus, the optical diode factor k represents the minimum diode factor an absorber can achieve, similar to the QFLS representing the maximum open circuit voltage an absorber is capable of, if the formation of the solar cell and the contacts do not introduce further losses.

As seen in figure 2, the main recombination mechanism in solar cell absorbers is non-radiative, i.e. SRH recombination. The non-radiative recombination rate is given by (see e.g. [78]):

$$r_{\mathrm{SRH}} = \frac{np - n_i^2}{\tau_p(n + n*) + \tau_n(p + p*)} \quad \text{with}$$
$$n*, p* = N_{C,V}\mathrm{e}^{\pm(E_T - E_{C,V})/k_B T}. \tag{13}$$

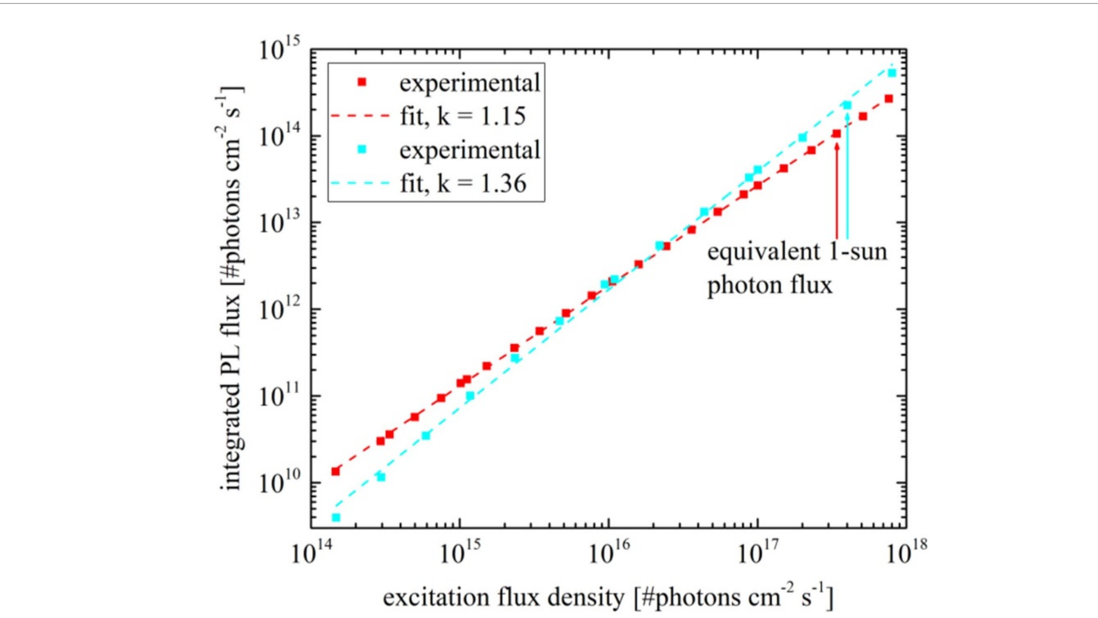

Figure 7. PL flux as a function of generation flux, demonstrating the power law dependence over four orders of magnitude for two different polycrystalline $Cu(In,Ga)Se_2$ samples. Reproduced from [30]. CC BY 4.0.

Table 1. Radiative and non-radiative recombination rates. For clarity we assume a p-type semiconductor. Furthermore we assume that the dominating recombination is non-radiative, i.e. $g = r_{tot} \approx r_{SRH}$. It should be noted that an undoped semiconductor is in the high excitation situation for any measureable excitation.

	Low excitation	High excitation
Recombination via deep recombination centre	$n = \Delta n, p = p_0$ $r_{SRH} = \frac{\Delta n}{\tau} \sim \Delta n\ \tau = \tau_n$ $F_{PL} = B\Delta np \sim \Delta n \sim g \Rightarrow k = 1$	$p = n = \Delta n$ $r_{SRH} = \frac{\Delta n}{\tau} \sim \Delta n\ \tau = \tau_n + \tau_p$ $F_{PL} = B(\Delta n)^2 \sim (\Delta n)^2 \sim g^2 \Rightarrow k = 2$
Recombination via tail states	$r_{SRH} = \frac{\Delta n}{\tau} \sim \Delta n$ $\tau = \tau_p \cdot \frac{n*}{p}$ or $\tau_n \cdot \frac{p+p*}{p}$ $F_{PL} = B\Delta np \sim \Delta n \sim g \Rightarrow k = 1$	$r_{SRH} = \frac{(\Delta n)^2}{\tau'} \sim (\Delta n)^2$ $\tau' = \tau_n \cdot p*$ or $\tau_p \cdot n*$ $F_{PL} = B(\Delta n)^2 \sim (\Delta n)^2 \sim g \Rightarrow k = 1$
With metastable defects	$k = 1 + \frac{d(\ln p)}{d(\ln g)}$	No change to the above

We consider excited semiconductors, i.e. $np \gg n_i^2$. For a recombination centre deep in the gap and the semiconductor in the excited state $n^*, p^* \ll n, p$, whereas for a tail state and a non-degenerate semiconductor n^* or $p^* \gg n, p$, depending on whether we consider a conduction band or a valence band tail. Therefore in equation (13) several of the terms in the sum of the denominator can be neglected. Furthermore, in the case of low excitation by definition $n_{min} \ll n_{maj}$, whereas in the case of high excitation: $n = p$. With these simplifications we can distinguish the four cases in table 1. Furthermore the generation rate is equal to the total recombination rate, which is dominated by the non-radiative recombination: $g \approx r_{SRH}$. It should be noted that these considerations neglect the potential interaction with additional defects, which capture carriers from the bands, which then can recombine (radiatively) from the defect. In that case all the individual capture and recombination rates have to be considered simultaneously [79]. However, at room temperature the carriers are reexcited into the band and SRH recombination will give the correct recombination rates, as given in table 1.

The optical diode factor is defined by equation (11) and can therefore be written as:

$$k = \frac{d(\ln F_{PL})}{d(\ln G)} = \frac{d(\ln n)}{d(\ln g)} + \frac{d(\ln p)}{d(\ln g)}. \tag{14}$$

From table 1 it is obvious, that with SRH recombination through deep defects or through tail states, the optical diode factor in low excitation should be 1 in either case. Only in the case of high excitation and deep defect recombination, is the optical diode factor expected to be 2. This can be understood by the fact, that in low excitation only the minority carrier Fermi level moves closer to the band with increasing excitation, therefore the first term in equation (14) is 1 and the second term is 0, leading to $k = 1$. In the high excitation case, both Fermi levels move, thus both terms in equation (14) are 1, leading to $k = 2$. Interestingly, in the

case of high excitation but recombination through tail states both Fermi levels move, but not according to $\Delta n \sim g$, but according to $\Delta n = \sqrt{g}$, thus both terms in equation (14) are 1/2, leading to an optical diode factor of 1. Furthermore, at high excitation radiative recombination will become dominant. Based on detailed balance arguments [79], both terms in equation (14) become 1/2, and the optical diode factor $k = 1$ at high enough excitation. For a simulation of the optical diode factor for the various cases see [30]. Here, we ignore the effect of Auger recombination, which could become important at high excitation [5].

Experimentally, however, in the low excitation case, where $k = 1$ is expected, we observe considerably larger optical diode factors, typically ranging from 1.2 to 1.3 [64]. This effect can be explained by metastable defects, which change their character from donor to acceptor upon electron capture, i.e. upon excitation [30]. Such metastable defects are well known in chalcopyrite materials [80–82], but also in other semiconductors (see references in [30]). In chalcopyrites one of the main metastable effects can be explained by a donor effect, that turns into an acceptor upon electron capture, e.g. due to illumination [80–82]. Consequently the effective p-doping increases upon illumination, and the increase depends on the available minority carrier concentration. Thus, the majority quasi Fermi level shifts, but not in direct dependence of the generation, but in dependence of the minority carrier concentration, leading to an optical diode factor larger than 1. This has been confirmed by numerical simulations, as well as by experimental measurements of the net doping level after illumination [30]. Therefore metastable defects have a direct influence on the efficiency of solar cells via the diode factor. PL provides the optical diode factor and thus the best diode factor that can be achieved in a solar cell made from the corresponding absorber.

7. Summary

We summarise various ways how PL can be used to establish the maximum open circuit voltage and the lowest diode factor, i.e. highest fill factor, of a solar cell made from the same absorber. Absolute calibrated PL provides photon flux spectra, which can be fitted to extract the QFLS. The spectrally integrated flux gives the ERE, which can also be used to determine the QFLS via equation (7). Once the QFLS is known, the PL spectrum allows the determination of the absorption spectrum, down to very low absorption coefficients, which is the ideal tool to measure tails states in the band gap. These tail states reduce QFLS and V_{OC} due to an increase of radiative recombination at lower energies and due to non-radiative recombination via the tail states. This loss is significant: every meV increase in the Urbach energy reduces QFLS, and thus the V_{OC}, by at least 10 meV. In non-optimised devices often the observed V_{OC} is much smaller than $\Delta E_F/q$ by several 100 mV. This additional loss indicates interface recombination, caused by non-ideal electronic structure at the interface: (a) the band alignment at the absorber-contact interface forms a cliff, (b) the interface has a very high density of defects states, which pin the Fermi level, (c) the surface of the absorber consists of a highly defective layer. Besides these limitations for the open circuit voltage, PL can also make predictions concerning the fill factor of the solar cell. An increased diode factor decreases the fill factor. The diode factor of the absorber alone can be measured by intensity dependent PL. The exponent of the power law is the optical diode factor. Metastable defects can cause an increase of the diode factor, even for recombination in the neutral zone and under low excitation.

Data availability statement

The data that support the findings of this study are openly available at the following URL/DOI: 10.5281/zenodo.5145859 [83].

Acknowledgments

We gratefully acknowledge the financial support by the Luxembourgish Fond National de la Recherche (FNR), in the framework of the projects MASSENA (PRIDE 15/10935404/MASSENA), CorrKest (C15/MS/10386094/ CORRKEST) and GRISC (C17/MS/11696002 GRISC), as well as by the European Union's Horizon 2020 research and innovation program in the framework of the Sharc25 project (Grant No. 641004). For the purpose of open access, the author has applied a Creative Commons Attributions 4.0 International (CC BY 4.0) license to any Author Accepted Manuscript version arising from this submission.

We would like to thank Dr Venkatesh Tunuguntla for help in preparing figure 2.

Annex

List of symbols

Var.	Meaning	Units, typically
V	Voltage	V
V_{OC}	Open circuit voltage	
V_{OC}^{SQ}	In the Shockley–Queisser case	
V_{OC}^{rad}	Limited only by radiative recombination in the case of tail states	
ΔV_{OC}^{IF}	Interface open circuit voltage loss	
ΔE_F	Quasi Fermi level splitting	eV
Φ	Spectral photon flux	$1\ (\mathrm{cm^2\ s\ eV})^{-1}$ all our spectra are in function of E
Φ_{eq}	In equilibrium	
Φ_{BB}	Black body	
Φ_{PL}	Photoluminescence	
E	Energy	eV
E_G	Band gap	eV
A	Absorptance	1
T	Temperature	K
F	Integrated photon flux	$1\ (\mathrm{cm^2\ s})^{-1}$
F_{eq}	Equilibrium	
F_{PL}	Photoluminescence	
F_{nr}	Flux loss due to non-radiative recombination	
B^*	**Flux** radiative recombination coefficient, similar to the Einstein coefficient, which describes the recombination **rate**	$\mathrm{cm^4\ s^{-1}}$
p	Hole concentration	$\mathrm{cm^{-3}}$
n	Electron concentration	
n_i	Intrinsic carrier concentration	
n_{min}	Minority carrier concentration	
n_{maj}	Majority carrier concentration	
Δn	Photo generated carrier concentration	
ERE	External radiative efficiency	1
EQE	External quantum efficiency (of the short circuit current)	1
G_{sun}	Integrated excitation flux from the sun	$1\ (\mathrm{cm^2\ s})^{-1}$
G	Generation flux in a PL measurement	
τ	Minority carrier lifetime	s
τ_p	SRH lifetime for holes	
τ_n	SRH lifetime for electrons	
d	Absorber thickness	m
j	Current density	$\mathrm{A\ cm^{-2}}$
j_{SC}	Short circuit current density	
j_0	Reverse saturation current density	
j_{00}	Prefactor of the reverse saturation current density	
E_a	Activation energy of the reverse saturation current	eV
n_d	Diode factor	1
k	Optical diode factor	1
r_{SRH}	Shockley–Read–Hall recombination rate	$\mathrm{cm^{-3}\ s^{-1}}$
r_{tot}	Total recombination rate	
g	Generation rate	$\mathrm{cm^{-3}\ s^{-1}}$
n^*, p^*	Auxiliary electron or hole concentration in SRH recombination	
$N_{C,V}$	Effective density of states of the conduction or valence band	$\mathrm{cm^{-3}}$
$E_{C,V}$	Energy of conduction or valence band edge	eV
E_T	Energy of state in band gap	

Constants	Meaning
q	Elementary charge
$\hbar$	Reduced Planck constant
c	Vacuum velocity of light
k_B	Boltzmann constant

ORCID iDs

Susanne Siebentritt https://orcid.org/0000-0001-6522-1427
Alberto Lomuscio https://orcid.org/0000-0002-3356-2486

References

[1] UNEP 2016 Green energy choices: the benefits, risks and trade-offs of low-carbon technologies for electricity production *Report of the International Resource Panel* ed E G Hertwich, J Aloisi de Larderel, A Arvesen, P Bayer, J Bergesen, E Bouman, T Gibon, G Heath, C Peña, P Purohit, A Ramirez and S Suh *et al* (available at: https://www.unep.org/resources/report/green-energy-choices-benefits-risks-and-trade-offs-low-carbon-technologies)
[2] Green M, Dunlop E, Hohl-Ebinger J, Yoshita M, Kopidakis N and Hao X J 2021 *Prog. Photovolt., Res. Appl.* **29** 3
[3] Nakamura M, Yamaguchi K, Kimoto Y, Yasaki Y, Kato T and Sugimoto H 2019 Cd-free Cu(In,Ga)(Se,S)2 thin-film solar cell with record efficiency of 23.35% *IEEE J. Photovolt.* **9** 1863
[4] Jeong M *et al* 2020 *Science* **369** 1615
[5] Kirchartz T, Márquez J A, Stolterfoht M and Unold T 2020 *Adv. Energy Mater.* **10** 1904134
[6] Shockley W and Queisser H J 1961 *J. Appl. Phys.* **32** 510
[7] Rau U, Blank B, Müller T C and Kirchartz T 2017 *Phys. Rev. Appl.* **7** 044016
[8] Rau U, Huhn V and Pieters B E 2020 *Phys. Rev. Appl.* **14** 014046
[9] Würfel P 1982 *J. Phys. C: Solid State Phys.* **15** 3967
[10] Würfel P 2005 *Physics of Solar Cells* (Weinheim: Wiley-VCH)
[11] Gütay L and Bauer G H 2007 *Thin Solid Films* **515** 6212
[12] Gütay L and Bauer G H 2009 *Thin Solid Films* **517** 2222
[13] Unold T and Gütay L 2011 *Advanced Characterization Techniques for Thin Film Solar Cells* ed D Abou-Ras, T Kirchartz and U Rau (New York: Wiley) p 151
[14] Babbe F, Choubrac L and Siebentritt S 2016 *Appl. Phys. Lett.* **109** 082105
[15] Rey G, Spindler C, Babbe F, Rachad W, Siebentritt S, Nuys M, Carius R, Li S and Platzer-Björkman C 2018 *Phys. Rev. Appl.* **9** 064008
[16] Rühle S 2016 *Sol. Energy* **130** 139
[17] Yu P and Cardona M 2010 *Fundamentals of Semiconductors* (Berlin: Springer) p 398
[18] Rey G, Redinger A, Sendler J, Weiss T P, Thevenin M, Guennou M, Adib B E and Siebentritt S 2014 *Appl. Phys. Lett.* **105** 112106
[19] Carron R *et al* 2019 *Thin Solid Films* **669** 482
[20] Miller O D, Yablonovitch E and Kurtz S R 2012 *IEEE J. Photovolt.* **2** 303
[21] Siebentritt S *et al* 2020 *Adv. Energy Mater.* **10** 1903752
[22] Wolter M H, Bissig B, Avancini E, Carron R, Buecheler S, Jackson P and Siebentritt S 2018 *IEEE J. Photovolt.* **8** 1320
[23] Lomuscio A, Rödel T, Schwarz T, Gault B, Melchiorre M, Raabe D and Siebentritt S 2019 *Phys. Rev. Appl.* **11** 054052
[24] Rau U 2007 *Phys. Rev.* B **76** 085303
[25] Wolter M 2019 *Doctoral Thesis* University of Luxembourg (available at: https://orbilu.uni.lu/handle/10993/39611) (Accessed 01 September 2021)
[26] Green M A, Hishikawa Y, Warta W, Dunlop E D, Levi D H, Hohl-Ebinger J and Ho-Baillie A W H 2017 *Prog. Photovolt., Res. Appl.* **25** 668
[27] Green M A, Emery K, Hishikawa Y, Warta W and Dunlop E D 2012 *Prog. Photovolt., Res. Appl.* **20** 606
[28] Ross R T 1967 *J. Chem. Phys.* **46** 4590
[29] Ganapati V, Steiner M A and Yablonovitch E 2016 *IEEE J. Photovolt.* **6** 801
[30] Weiss T P, Ehre F, Serrano-Escalante V, Wang T and Siebentritt S 2021 *Sol. RRL* **5** 2100063
[31] Adeleye D, Lomuscio A, Sood M and Siebentritt S 2021 *Mater. Res. Express* **8** 025905
[32] Maiberg M, Hölscher T, Zahedi-Azad S and Scheer R 2015 *J. Appl. Phys.* **118** 105701
[33] Maiberg M and Scheer R 2014 *J. Appl. Phys.* **116** 123711
[34] Maiberg M and Scheer R 2014 *J. Appl. Phys.* **116** 123710
[35] Werner F 2017 *J. Appl. Phys.* **122** 135306
[36] Gunawan O *et al* 2019 *Nature* **575** 151
[37] Blood P and Orton J W 1992 *The Electrical Characterization of Semiconductors: Majority Carriers and Electron States* (New York: Academic)
[38] Heath J and Zabierowski P 2011 *Advanced Characterization Techniques for Thin Film Solar Cells* ed D Abou-Ras, T Kirchartz and U Rau (Weinheim: Wiley-VCH) pp 81–102
[39] Siebentritt S, Rey G, Finger A, Regesch D, Sendler J, Weiss T P and Bertram T 2016 *Sol. Energy Mater. Sol. Cells* **158** 126
[40] Sumi H and Toyozawa Y 1971 *J. Phys. Soc. Japan* **31** 342
[41] Kurik M V 1971 *Phys. Status Solidi* a **6** 9
[42] Skettrup T 1978 *Phys. Rev.* B **18** 2622
[43] Johnson S R and Tiedje T 1995 *J. Appl. Phys.* **78** 5609
[44] Urbach F 1953 *Phys. Rev.* **92** 1324
[45] Cody G D, Tiedje T, Abeles B, Brooks B and Goldstein Y 1981 *Phys. Rev. Lett.* **47** 1480
[46] Ayik C, Studenyak I, Kranjec M and Kurik M 2014 *Int. J. Opt. Appl.* **4** 76
[47] Rey G, Larramona G, Bourdais S, Choné C, Delatouche B, Jacob A, Dennler G and Siebentritt S 2018 *Sol. Energy Mater. Sol. Cells* **179** 142
[48] Werner J H, Mattheis J and Rau U 2005 *Thin Solid Films* **480–81** 399
[49] Yu P W 1977 *J. Appl. Phys.* **48** 5043
[50] Siebentritt S, Papathanasiou N and Lux-Steiner M C 2006 *Physica* B **376–77** 831
[51] Larsen J, Burger K, Gütay L and Siebentritt S 2011 *37th IEEE Photovoltaic Specialist Conf.* (*Seattle: IEEE*) p 396
[52] Wright A D, Milot R L, Eperon G E, Snaith H J, Johnston M B and Herz L M 2017 *Adv. Funct. Mater.* **27** 1700860
[53] Gislason H P, Yang B H, Pétursson J and Linnarsson M K 1993 *J. Appl. Phys.* **74** 7275
[54] Shklovskii B I and Efros A L 1984 *Electronic Properties of Doped Semiconductors* (Berlin: Springer)
[55] Jackson W B and Amer N M 1982 *Phys. Rev.* B **25** 5559

[56] Vanecek M, Kocka J, Stuchlik J and Triska A 1981 *Solid State Commun.* **39** 1199
[57] Daub E and Würfel P 1995 *Phys. Rev. Lett.* **74** 1020
[58] Jackson W B, Amer N M, Boccara A C and Fournier D 1981 *Appl. Opt.* **20** 1333
[59] Pankove J I 1975 *Optical Processes in Semiconductors* (New York: Dover Publications)
[60] Wolter M H *et al* 2021 *Prog. Photovolt.* (https://doi.org/10.1002/pip.3449)
[61] Weiss T P, Bissig B, Feurer T, Carron R, Buecheler S and Tiwari A N 2019 *Sci. Rep.* **9** 5385
[62] Scheer R and Schock H W 2011 *Chalcogenide Photovoltaics: Physics, Technologies, and Thin Film Devices* (Weinheim: Wiley-VCH)
[63] Stolterfoht M *et al* 2019 *Energy Environ. Sci.* **12** 2778
[64] Babbe F, Choubrac L and Siebentritt S 2018 *Sol. RRL* **2018** 1800248
[65] Sood M, Urbaniak A, Boumenou C K, Elanzeery H, Babbe F, Werner F, Melchiorre M, Redinger A and Siebentritt S 2021 *Prog. Photovolt.* accepted
[66] Böer K W 1992 *Survey of Semiconductor Physics II: Barriers, Junctions, Surfaces and Devices* (New York: Van Nostrand Reinhold)
[67] Rau U and Schock H W 1999 *Appl. Phys.* A **69** 131
[68] Kim S, Nagai T, Tampo H, Ishizuka S and Shibata H 2020 *Prog. Photovolt., Res. Appl.* **28** 816
[69] Elanzeery H, Melchiorre M, Sood M, Babbe F, Werner F, Brammertz G and Siebentritt S 2019 *Phys. Rev. Mater.* **3** 055403
[70] Sood M, Bombsch J, Shukla S, Lomuscio A, Wilks R G, Bär M and Siebentritt S 2021 Under review
[71] Turcu M, Pakma O and Rau U 2002 *Appl. Phys. Lett.* **80** 2598
[72] Shukla S *et al* 2021 *Joule* **7** 1816
[73] Siebentritt S, Gütay L, Regesch D, Aida Y and Deprédurand V 2013 *Sol. Energy Mater. Sol. Cells* **119** 18
[74] Merdes S, Saez-Araoz R, Ennaoui A, Klaer J, Lux-Steiner M C and Klenk R 2009 *Appl. Phys. Lett.* **95** 3
[75] Nelson J 2003 *The Physics of Solar Cells* (Singapore: World Scientific)
[76] Schmidt T, Lischka K and Zulehner W 1992 *Phys. Rev.* B **45** 8989
[77] Trupke T, Bardos R A, Abbott M D and Cotter J E 2005 *Appl. Phys. Lett.* **87** 093503
[78] Pierret R F 1986 *Advanced Semiconductor Fundamentals* (Reading, MA: Addison-Wesley)
[79] Spindler C, Galvani T, Wirtz L, Rey G and Siebentritt S 2019 *J. Appl. Phys.* **126** 175703
[80] Rau U, Weinert K, Nguyen Q, Mamor M, Hanna G, Jasenek A and Schock H W 2001 *Mater. Res. Soc. Symp. Proc.* **668** H9.1
[81] Zabierowski P, Rau U and Igalson M 2001 *Thin Solid Films* **387** 147
[82] Lany S and Zunger A 2006 *J. Appl. Phys.* **100** 113725
[83] Siebentrit S, Weiss T P, Sood M, Wolter M H, Lomuscio A and Ramirez O 2021 Data for "Photoluminescence tells us about voltages, recombination and diode factors in solar cells" (available at: https://zenodo.org/record/5145859#.YVXSgH2xVaQ)